High resolution COD image analysis for health monitoring of reinforced concrete structures through inverse analysis

By I. M. Nazmul[1] and T. Matsumoto[2]

[1]Assistant Professor, Department of Civil Engineering, Presidency University, Plot 11A, Gulshan 2, Dhaka 1212, Bangladesh. E mail: islammn@presidency.edu.bd. Phone: 880-2-885 7617 (ext. 501). Fax: 880-2-885 7618 (ext. 200).

[2]Associate Professor, Department of Civil Engineering, the University of Tokyo, 7-3-1 Hongo, Bunkyo-Ku, Tokyo 113-8656, Japan. E mail: matsumoto@civil.t.u-tokyo.ac.jp Phone: 81-3-5841-6092. Fax: 81-3-5841-7496.

Abstract: Direct and inverse problems of a fracture mechanics based RC beam model are solved. Solution of the direct problem that maps crack bridging stresses into Crack Opening Displacements (COD) is straightforward, but the inverse problem is ill-posed, and better solved by the theory of inverse problems. This paper exploits the Tikhonov regularization method to solve the inverse problem, and estimates the force and location of rebar in buried concrete from CODs. Bending tests are carried out on model RC beams in the laboratory to demonstrate the applicability of the method. During the tests, a microscopic camera snaps high resolution digital pictures of cracked concrete surface. The images are analyzed by a software to measure surface CODs that are input into the

inverse problem. The practical CODs inevitably include noise due to experimental error, which makes the inverse problem ill-posed, and necessitates regularization. In the current inverse analysis by the Tikhonov Regularization method, bridging stress profiles, i.e. variation of the crack bridging stress along the crack length, has been figured out. Results are compared with those from other theoretical methods of analysis as well as with the readings from strain gauges. The method is a suitable non-destructive means for existing structures in cases where the section information is inadequate, or damages/repairs have altered the designed cross-section.

***Keywords**: Crack opening displacements, image analysis, inverse problem, regularization, rebar force.*

Introduction

Evaluation of physical and mechanical states of buried rebars is of keen interest for Structural Health Monitoring (SHM) and maintenance of RC structures. Recent constructions embed sensors (piezoelectric, fiber optics, etc.) at key locations for these purposes, without which aging infrastructure systems exhibit little information about their intrinsic deterioration, unless a Non-Destructive Test (NDT) is adopted where the response data due to an incited excitation are collected and processed (see ACI Committee report on NDT methods, 1998 and Chong et al., 2003 for recent SHM techniques). Without instrumental excitation and sensing, the only evidence of the internal stress states are numerous surface cracks. Dimensions, distributions, and profiles

of structural cracks depend on the geometry of a structure (external and cross-sectional), applied loading, and crack bridging mechanisms, along with stress states and material properties.

Fracture mechanics based integral transforms relate CODs with active and reactive stresses in closed forms (e.g. Cox and Marshall, 1991a), the inverse problems of which are capable of estimating the magnitude and distribution of crack bridging stress from CODs. A fracture mechanics based transformation between rebar stress and COD has been derived by Nazmul and Matsumoto (2003) for cracked RC beams, and a numerical method for the solution of the ill-posed inverse problem by the Tikhonov regularization method has been explained in Nazmul and Matsumoto (2004). This paper proposes a method based on image analysis to measure CODs on concrete surface, estimates rebar force and location from CODs through inverse analysis, and discusses the accuracy and applicability of the method.

Fracture mechanics based integral transforms between crack bridging stress and COD were derived by many researchers in the last several decades (e.g. Marshall et al., 1985, Cox and Marshall, 1991a, Fett et al., 1996). Those computations were focused on ceramic matrix composites (CMC) or metal matrix composites (MMC) with extension to fiber reinforced concrete (FRC) and plain concrete (Kitsutaka, 1997). Most of those computations worked on the direct problems of estimating CODs from the known external loadings and assumed crack bridging stresses. Buchanan et al. (1997) used the

finite element method to determine the crack bridging stresses from the CODs in CMC or MMC.

Cox and Marshall (1991b) addressed the ill-posedness of the inverse problem in cases of continuously aligned fiber composites, and devised a solution based on the Tikhonov regularization method to estimate crack bridging stress from CODs. Results presented by them used only synthetic COD data, and Massabo et al. (1998) went further ahead with both synthetic and practical CODs to characterize the bridging mechanisms developed across delamination cracks by through-the-thickness reinforcements under mode II loading. This paper narrates the bending tests on model RC beams, explains a method of image collection and analysis to measure surface CODs, reformulates the basic equations of the Tikhonov regularization method [Tikhonov et. al. 1990] to fit into RC beam bending, and estimates the rebar force from the practical CODs.

Cracked RC beam model

A two dimensional bridged crack model is assumed for a through-the-thickness cracked RC beam, after the crack has passed all rebar layers. Linear elastic behavior of rebar and concrete is assumed at this stage, after an initial slip of rebars has occurred at crack initiation. These assumptions restrict the application of the current model within the loading interval between crack initiation (initial slippage) and rebar yielding, marked as the service loading range in Fig. 3. Progressive debonding between steel and concrete is accounted for by another rigid-plastic bond-slip law, discussed in Appendix A. Cracked RC beams of similar geometry were modeled by Carpinteri (1984), Bosco and Carpinteri

(1992), and Carpinteri (1991) to examine fracture behavior in flexure. They also adopted a bridged crack model to examine the influence of rebars on a crack in the matrix at different stages of rebar behavior. Results presented by them include applied bending moments corresponding to fracture initiation in concrete, and yield initiation to the rebars. Carpinteri and Massabo (1997) took a novel approach by proposing nonlinear fracture mechanics models, which describe constitutive flexural behavior of brittle-matrix composites with localized and distributed ductile reinforcements.

Following the procedures described in Cox and Marshall (1991a), and simulating rebar force as shown in Fig. 1, Nazmul and Matsumoto (2003) derived COD profiles, $u(x)$ of RC beams under an applied (bending) stress $\sigma(x)$ on the crack plane, which for the case of plane strain is

$$u(x) = \frac{4(1-\nu^2)}{E_c}\int_x^a \left[\int_0^{a'} G(x',a',b)[\sigma(x') - f(x')]dx'\right] G(x,a',b)da' \qquad (1)$$

where E_c and ν are the Young's modulus and the Poisson's ratio of concrete respectively, and a is the crack length. $G(x,a,b)$ is the weight (influence) function for a particular crack geometry, standard forms of which are available for a large variety of geometry in stress intensity handbooks (Tada et al., 1985). b is the beam total depth and x', a' are the dummy variables for x, a. The term $f(x')$ in Eq. (1) is the rebar force, considered as force per unit length along the crack (Fig. 1), which must be integrated over the cracked domain to obtain the total rebar force F for an acting bending moment M as

$$\int_0^a f(x)dx = F = \frac{M}{j\,d}. \tag{2}$$

jd is the internal lever arm between the total tension force in the rebar, and the total compression force in concrete, as simulated in the flexural analysis of cracked RC beam cross-section [Nilson et al., 2003], where d is the effective beam depth. The transformation of a point rebar force into a distributed force per unit length $f(x)$ is mathematically simulated by Unit Step Functions for any (m) number of rebar layers as (Nazmul and Matsumoto, 2004)

$$f(x) = \sum_{i=1}^{m} f_i \left[H(x - h_i) - H(x - h_i - d_{b_i}) \right] \tag{3}$$

where, by $f_i = (F_i / d_{b_i})$ the point loads of rebars are converted into (stepped) line loads (Fig. 1) along the crack, F_i is the total force at the i-th layer where the rebar diameter is d_{b_i}, and h_i is the clear distance of a layer from the bottom face. It should be noted that cracks are usually meandering , which renders a non-linear x coordinate, but in this study linearity is ascertained by measuring x at regular intervals along the crack plane, and CODs normal to the x direction.

Results shown in this paper are two-fold. First, practical CODs on a cracked RC beam surface under a constant load are measured by image analysis, and presented in Fig. 6. For comparison, practical CODs are plotted with the theoretical one's obtained by the direct solutions of Eq. (1). But, the direct solution requires a known rebar force, which in turn, requires the known cross-section of a beam. Since all information was available

during the laboratory tests, Eq. (2) was applied to determine the rebar force, and the theoretical CODs were calculated by directly solving Eq. (1). Later, the cross-section will be considered unknown in the inverse analysis, and only CODs will be used to estimate the rebar force.

The second set of results presented in Fig. 7 is the set of rebar forces estimated by the inverse analysis of practical and theoretical CODs. Only CODs and the applied load are required here without any cross-section information, which manifests the applicability of the proposed method to the existing structures. A further insight into Fig. 7 reveals that noiseless theoretical CODs yielded the exact rebar force (dotted lines), which demonstrates the correctness of the mathematical procedure. Better approximations from practical CODs are obtained by minimizing errors in COD measurements, convergence during numerical approximations, and on a correct choice of the regularization parameter.

The laboratory test

Materials and specimens

A batch of eight RC beams was cast in the laboratory with normal strength concrete and steel rebars deformed with lateral ribs. All beams were 40 cm long with 10 cm x 10 cm uniform square cross-section (Fig. 2). By compressive tests on 10 cylindrical test specimens of dimensions 10 cm x 20 cm the average compressive strength of the concrete was determined to be 30 MPa. The yield strength of the rebar was determined to be 345 MPa. For these values a balanced steel reinforcement proportion of 0.0293 can be

computed. The reinforcement ratios of the model beams were kept less than this value by placing only two 6 mm diameter rebars in order to obtain comprehensive crack propagation before steel yielding. The clear covers at the bottom were varied (25 mm to 35 mm) among the specimens to examine appropriateness in determination of location of rebars, whereas the side covers were 20 mm on both sides for all specimens. The specimens were cured in the laboratory for 28 days before testing.

A concrete cutter with a 1 mm thick cutter blade was used to create 3 mm wide notches of 1 cm depth at middle of the bottom faces of all specimens. The notch ensures that the crack plane will be right at the middle. The front and back faces of the specimens were painted white to make adequate contrast between cracked and non-cracked zones.

Electrical resistance strain gauges were attached on rebar's surfaces, at 3 cm inward from the possible crack plane at the notch. Required areas on the rebar's surfaces were smoothened by sand paper for better adherence, and strong adhesives were used. Strictly speaking, the strain gauges should be attached at the midspan over the notch, since their readings will be compared with the estimated rebar force at the cracked section. But progressive cracking in concrete and subsequent friction at steel-concrete interface lead to unreliable strain gauge reading, or even damage of the gauges. Alternatively, attachment of strain gauges 3 cm inward from the crack plane leads to underestimation of the rebar strain, because concrete carries a significant tensile stress at the uncracked section. A "strain correction" has been introduced to amend this error, which is explained in Appendix A.

Test procedure

Four-point static bending tests were carried out by a digital electro-hydraulic feed-back controlled universal testing machine. Displacement control was selected, while the load, the mid-span deflection, and the rebar strain histories were recorded. Sample test data showing total load vs. rebar strains are shown in Fig. 3. The theoretical strains in Fig. 3 were computed by the elastic flexure formula while the section remains uncracked, and by Eq. (2) after the section has been cracked. The comparison of strain gauge readings with the theoretical strains demonstrates that the strain histories recorded by the strain gauges were expected, particularly the load plateau, when the rebar force experiences a jump as the tensile stress at the bottom exceeds the modulus of rupture, taken as $7.5\sqrt{f_c'}$ [Nilson et al., 2003]. As the crack propagates with increasing bending moment beyond the "load plateau", rebar stresses are linear elastic until the steel yields, as predicted by the theoretical strains as well as evidenced by the strain gauge readings (Fig. 3). The interval between crack initiation and steel yielding is the service loading range, where the current model is applicable. Monotonic loading was interrupted several times within this interval, suspended for approximately 6 minutes while the microscope was allowed to take pictures under a constant load, after which loading had been resumed.

Collection of Images

The laboratory set-up consisted of a microscopic digital camera, and a 3-axis controlled stage system (Fig. 4), both having separate controller units, synchronized and operated by a computer. The set-up had been mounted in front of the beam specimen before any load was applied, and no out-of-plane movement was allowed after focus and accommodation of the lens. A 4 cm x 10 cm area having the notch at the middle was marked on the beam

front face. The area was virtually divided into a grid by 21 horizontal and 9 vertical straight lines, all with 5 mm spacing. Thus the grid had 189 points of intersection, to be focused by the microscope. The microscope focused on a point, took a picture covering 6.67 mm x 5 mm area with the point at the centroid, stored the picture into a 640 x 480 pixel image file of 2400 dpi, and moved to the following point. Starting from the top-right, the image capturing process finished at the bottom-left corner, and the microscopic lens automatically moved back to the top-right corner for the next set of images.

Image analysis

The digital images contained cracked beam surface information in terms of pixel values (e. g. RGB values), exploited in the image analysis method to determine CODs. Image analysis methods for COD measurements have been reported in literature by many researchers of material science and engineering. For example, small-scale CODs in CMC or MMC are determined by Scanning Electron Microscopes (SEM), or Laser Interferometric Displacement Gauges (IDG) (Buchanan et al., 1997, Rodel et al., 1990). A video microscope in combination with an automated image analysis was reported by Schutter (2002) for crack width measurement. In this study, gray value variation among the pixels along an arbitrary line was exploited to measure CODs.

Gray value measures the intensity of light at a pixel, defined by a series of shades from white to black, with a value 255 for white, and a zero for black. A schematic explanation of the procedure of measuring COD is shown in Fig. 5, where a continuous profile of gray value variation (Fig. 5c) along a line AB was evaluated. It was observed that the gray values were almost white (since the beam surface was painted white) at all pixels,

except the crack proximity, where gray values sharply decreased at the crack boundary, reached a minimum at the crack plane, and again sharply increased at the other boundary. The actual crack boundaries were assumed at the mid-heights of the cliffs of the gray value profile, and CODs were measured as shown in Fig. 5. Measurement of CODs started from the crack mouth at $x = 0$, proceeded along the crack plane on equal interval h_x up to the crack tip at $x = a$, and a COD profile was obtained as

$$(x,u) = \{(x_k, u_k), k = 1,....., p\} \text{ with } x_1 = 0 \text{ and } x_p = a. \quad (4)$$

COD profiles

Practical COD profiles

Practical COD plot points along the crack are shown in Fig. 6 as dots. Local fluctuations in the raw COD data were smoothened by a linear filter. The linear filter with weights $\{c_0, c_1, c_2, ..., c_r\}$ transformed the obtained COD data to weighted average as

$$\sum_{j=0}^{r-1} c_j u_{t-j} \text{ for } t = r, r+1, ..., p \quad (5)$$

where, the total number of data points were reduced to $n - r + 1$. Here, the weights in the linear filter were so chosen that $\sum_{j=0}^{r-1} c_j = 1$, which is called a simple moving average. Smoothened COD profiles are shown in Fig. 6 as solid lines.

Location of rebars was primarily identified at the depression of a COD profile. A series of depressions are expected for several layers of rebars [Nazmul and Matsumoto, 2003], which, for a wider grid, may merge into one long depression. Such a long depression in the COD profile is also a viable input for the inverse analysis to obtain the total rebar force, since adoption of a finer grid should be compromised with computation time and efficiency. Another way is to have more data points at rebar locations, which has been followed in this study. CODs were measured in a grid having $h_x = 0.1\text{mm}$ at suspected rebar locations, and $h_x = 1\text{mm}$ at other locations. The rest CODs are interpolated for the smaller grid.

The reason of tortuousness of the COD profiles is the inherent roughness of the fracture surfaces, which depends primarily on the size and type of aggregates, existence of impurities or voids, heterogeneity in compaction, etc. Apparent noise in the practical CODs due to these reasons are assumed to be successfully mitigated by the linear filter. But, fracture surface roughness is not the only source of noise in the data. Approximations and assumptions during image collection and analysis invoke more errors in COD data for which regularization is needed.

Theoretical COD profiles

If the rebar force was calculated by a cracked RC beam section analysis (which uses the cross-section geometry) using Eq. (2), the direct solution of Eq. (1) would yield the other COD profiles of Fig. 6. Analytical COD profiles are the solutions of the definite integrals of Eq. (1) by symbolic calculations. But, the inverse problem cannot be solved symbolically since CODs at grid-points are to be measured and entered. That's why Eq.

(1) is cast into its numerical form by replacing all functions with their finite difference equivalent vectors or matrices. The direct solutions of the numerical forms of Eq. (1) yielded the numerical COD profiles of Fig. 6. The comparison between the analytical and the numerical COD profiles demonstrates the convergence of functions while being replaced by their finite difference equivalents in a pre-defined grid; the finer the grid, the better the convergence. The large deviation of analytical/numerical COD profiles from the experimental one is primarily due to neglecting bond-slip behavior of rebar in the model, discussed in Appendix A, and secondarily, due to idealization of the three dimensional beam into a two dimensional one, neglecting the effects of concrete cover, due to which centerline CODs are amplified at the surface.

However, Eq. (1) is an integral transform as a direct problem. The results of the inverse problem are sensitive to the gradient of a COD profile, and more specifically, to the depressions at rebar locations. It is assumed that disregard of the effects of bond-slip and concrete cover underestimates the absolute COD values, but approximates the gradient of a COD profile within tolerable noise level, to be successfully mitigated by the Tikhonov regularization method. This is further supported by the facts that no stress relaxation occurs due to slip, and the rebar force remains the same before and after slip under a constant external loading.

In addition, due to the heterogeneity of concrete, and a possible three-dimensional stress state along the crack front, a reverse channel shape of a crack profile is observed along the thickness of the beam, which overestimates the crack length (Jenq and Shah, 1991) as

manifested in Fig. 6 by different locations of crack tips. Theoretically, the location of a crack tip was obtained by the fracture condition of a bridged crack model,

$$K_{Ia} - K_{Ib} = K_{IC} \tag{6}$$

where, K_{Ia} and K_{Ib} are the stress intensity factors due to the external load and the crack bridging stress (rebar force) respectively, and K_{IC} is the fracture toughness of concrete (see Sauoma et al., 1982 for details). Practically obtained crack lengths are longer by a small percentage, which will underestimate the rebar force in inverse analysis as compared with other fracture mechanics based calculations.

Inverse analysis

Regularization of the inverse problem

To apply the Tikhonov regularization method of linear ill-posed problems, the net COD estimated by Eq. (1) is thought to be composed of two effects. First, the crack is opened due to an applied load with the profile $u_a(x)$, and second, the reactive rebar force closes the crack by $u_b(x)$ as

$$u(x) = u_a(x) - u_b(x) \tag{7}$$

where

$$u_a(x) = \frac{4(1-\nu^2)}{E_c} \int_x^a \left[\int_0^{a'} G(x', a', b)\sigma(x')dx' \right] G(x, a', b)da' \tag{8}$$

$$u_b(x) = \frac{4(1-\nu^2)}{E_c} \int_x^a \left[\int_0^{a'} G(x', a', b) f(x') dx' \right] G(x, a', b) da' . \quad (9)$$

The former part $u_a(x)$ may be determined for any known external loading within a grid of p points as

$$u_a := \{ u_{a_k}, k = 1, ..., p \} . \quad (10)$$

As such, data points relevant to the left side of Eq. (9) are determined by subtracting u of Eq. (4) from u_a of Eq. (10) as

$$u_b := \{ u_{b_k}, k = 1, ..., p \} = u_a - u \quad (11)$$

But, experimental CODs in Eq. (4) contain errors, where an incorrect u^δ is obtained instead of a correct u. Consequently u_b is perturbed as u_b^δ up to a noise level δ. We consider Eq. (9) as a linear operator equation $T : Z \to U$ between Hilbert spaces, which maps the rebar force $f \in Z$ into crack closings $u_b \in U$, and we adopt the Tikhonov regularization method, where the extremals of the following functional are sought

$$M^\alpha [f] = \left\| T_h f - u_b^\delta \right\|_U^2 + \alpha \| f \|_Z^2 . \quad (12)$$

T_h is the numerical approximation of the transformation T, and $\alpha > 0$ is the regularization parameter. A detailed method for solving the inverse problem of Eq. (9) is available in Nazmul and Matsumoto (2004), and a general mathematical procedure with

various examples is explained in Tikhonov et al. (1990). Finally, we reach a normal equation

$$\mathbf{B}\,\boldsymbol{f} + \alpha \mathbf{C}\,\boldsymbol{f} = \boldsymbol{v} \tag{13}$$

The matrix **C** is a $p \times p$ identity matrix for the linear spaces chosen as $Z, U \subset L_2(0, a)$, while the matrix **B** and the vector **v** have entries given by

$$B_{lj} = h_x \sum_{k=1}^{p} \left(\sum_{i=1}^{p} g_{li} g_{ki} \right) \left(\sum_{i=1}^{p} g_{ji} g_{ki} \right) \in \mathbf{B} \tag{14}$$

$$v_l = \sum_{k=1}^{p} \left(\sum_{i=1}^{p} g_{li} g_{ki} \right) u_{b_k}^{\delta} \in \mathbf{v}\,. \tag{15}$$

The weight function G for a Single Edge Notched fracture specimen is given in Appendix B. For numerical computations, G is approximated by its finite difference equivalent tensor, entries of which are found within the current grid as

$$\left.\begin{array}{ll} g_{ij} = G(x_i, a_j), & i = 2, \ldots\ldots, p-1 \\ g_{ij} = \dfrac{G(x_i, a_j)}{2}, & i = 1, p \end{array}\right\} \quad j = 1, \ldots, p\,. \tag{16}$$

Determining rebar location and force

Solutions of Eq. (13) are the vectors $\boldsymbol{f}$ corresponding to current grid of p points, which are shown in Fig. 7 as crack bridging stress profiles along the crack length. Each plot shows two sets of profiles, the solid and the dashed lines. The dashed lines estimate the exact rebar forces, but inputs CODs from the numerical COD profiles of Fig. 6. Machine generated random numbers of width 0.001 are added to those CODs to invoke noise, also

important to select a regularization parameter. On the other hand, the solid lines are the outputs of noisy practical CODs.

Location of the centroid of rebars is identified by the peak (point A), and the total rebar force is computed by the area under the bridging stress profiles. The profiles contain undulations due to noise in the data, which at some locations indicates existence of absurd negative crack bridging stresses. These undulations could be smoothed out using the statistical method presented earlier; nevertheless, the percentages of errors of unsmoothed curves are calculated to demonstrate the accuracy of the inverse analysis.

Accuracy of the inverse analysis method is checked in two ways (Table 1), (i) by comparing the estimated rebar force of inverse analysis with that obtained from other theoretical methods of analysis, and (ii) by comparing the estimated rebar strain by inverse analysis with that obtained by the attached strain gauges.

One of the theoretical methods to estimate the rebar force has been introduced in Eq. (2), derived from a cracked RC beam section analysis. Another fracture mechanics based method has been borrowed from Bosco and Carpinteri (1992). Both methods require cross-section data, contrasting the current method. This demonstrates the non-destructive nature of the inverse analysis method, to be applied to the existing structures. Table 1 shows the computed rebar stresses as well as error percentages compared with different methods. It is interesting to observe that the computed rebar stresses by inverse analysis

fell in between those of the section analysis, and Bosco and Carpinteri's (1992) fracture analysis results.

Estimated rebar strains from the inverse analysis method are compared with the strain gauge readings in Table 1. A "strain correction" is required since the strain gauges were attached at 3 cm inward from the crack plane, which is an uncracked section. The strain correction is related to the significant amount of stress carried by concrete in an uncracked section, as calculated in Appendix A.

Sensitivity of Results

Choice of a regularization parameter

Theoretically, the regularization parameter α is chosen according to the following principle

$$\alpha \to 0 \qquad \text{as } \frac{(\delta + h)^2}{\alpha} \to 0 \tag{17}$$

where $\delta > 0$ is the noise level of the data, and h is the error due to approximation of the transformation such that $\|T_h - T\| \le h$ (Kirsch, 1996). Families of regularization strategies were fabricated for different values of α, and the value which yields the infimum of the approximated Tikhonov functional, T_h was taken. However, the data error δ was uncertain in image analysis; a rough estimate was made in the following way.

Experimentally obtained COD profiles were undulating, partly due to roughness of the crack surfaces (mitigated by the linear filter) and mostly due to the error in data collection and image analysis. The average smooth curves (least square fit) of COD profiles were determined discarding the possible rebar locations, and the deviation of each COD point from the smoothed curve is computed. In this procedure, δ is determined as

$$\delta = \frac{\left\| u^{\delta} - u^{l} \right\|}{\left\| u^{l} \right\|} \tag{18}$$

where u^{δ} are the COD points on raw profile, and u^{l} are those on the smoothed least square fit.

Uncertainty in material properties

Any uncertainty in the determination of Young's modulus or Poisson's ratio leads to major deviations in the results as the method makes use of Young's moduli of both concrete and steel (Cox and Marshall, 1991b). The Young's modulus generally does not change during the service lives of structures, except for the structures under severe conditions. Core sampling or other non-destructive evaluation can be rendered for evaluation of material properties in-situ.

However, accuracy in determination of location is not hampered as $f(x)$ shifts up or down due to errors in Young's modulus changing the total rebar force value only. In the

cases of higher reinforcement ratios in the longitudinal direction, the orthotropic Young's modulus suggested by Cox and Marshall (1991a) should be used for better accuracy.

Conclusion

A high resolution image collection and analysis method to measure CODs on concrete surface has been demonstrated by laboratory experiments. A fracture mechanics based model has been developed to theoretically estimate those CODs. Some adjustments have been suggested in the model for bond-slip behavior of the rebars close to the crack plane.

Practically obtained CODs have been exploited to estimate the rebar force in buried concrete. But the practical CODs deviate from predicted theoretical values due to fracture surface roughness, and errors in image collection and analysis. The Tikhonov method of regularization of the theory of inverse problems has been employed in its numerical form which addresses those errors, and computes the best approximated rebar force. Accuracy of all methods has been tested, and demonstrated throughout the paper.

Accuracy in measuring CODs mostly depends on the resolution of the digital pictures, the better the resolutions, the more accurate are the CODs. Accuracy in estimated rebar force depends on the accuracy of COD data, accuracy in prediction of material properties, and on a correct choice of regularization parameter. However, undulations in raw data and in inverse analysis results may be minimized by statistical data smoothing methods.

The uniqueness of the current method to estimate rebar force lies in the fact that it does not require cross-section parameters like clear cover, reinforcement ratio, etc. The method may be used for structural health monitoring purposes since it uses external loadings, and external crack geometry only. Again, it only requires collecting digital pictures of the cracked concrete surfaces, which does not necessitate suspension of operation and does not require heavy equipment.

Acknowledgements: This study was supported by the Obayashi Foundation, Japan.

Appendix A: Bond-slip behavior of deformed bar

Bond-slip behavior

The importance of incorporating bond-slip behavior of buried rebars in the fracture mechanics based models has been demonstrated by Bazant and Cedoline (1980), where the length of the debonded zone, L_s for deformed bars being pulled with bar stress σ_h^s is derived as

$$L_s = \frac{(1-\rho)}{\pi U_b'(1-\rho+n\rho)}\sigma_h^s \tag{19}$$

where ρ and n are the reinforcement ratio and the modular ratio respectively. U_b' is the ultimate bond force per unit length. For standard deformed bars $U_b' = 2.9\sqrt{f_c'}$ for bar spacing≥ 150 mm, and $U_b' = 2.3\sqrt{f_c'}$ for bar spacing < 150 mm where f_c' is in MPa.

The amount of local pull-out depends on the fracture mechanical properties of the rebar-concrete interface, and on the surrounding concrete. Frictional stress at the rebar-concrete interface is not uniform along the longitudinal z direction (Fig. 7) throughout the debonded length $(0 \le z \le L_s)$. It is maximum near the exit $(z = 0)$, and reduces to zero at the end of debonded length $(z = L_s)$.

In Fig. 8, it is assumed that stresses in steel and concrete respectively vary linearly from $(\sigma_h^s, 0)$ in the open portion to (σ_o^s, σ_o^c) at the end of the debonded zone as

$$\sigma^s(z) = \sigma_h^s - \frac{z}{L_s}\left(\sigma_h^s - \sigma_o^s\right) \tag{20}$$

$$\sigma^c(z) = \frac{\sigma_o^c}{L_s} z \tag{21}$$

The relative slip, u_s is the difference between the elongations of steel u^s and concrete u^c, given by

$$u_s = u^s - u^c \tag{22}$$

We take derivatives of both sides of Eq. (22) to obtain strains in steel, ε^s and strain in concrete, ε^c respectively and we use stress-strain relation as

$$\frac{du_s}{dz} = \frac{du^s}{dz} - \frac{du^c}{dz} = \varepsilon^s - \varepsilon^c = \frac{1}{E_s}\sigma^s(z) - \frac{1}{E_c}\sigma^c(z) \tag{23}$$

where E_s and E_c are the Young's moduli of steel and concrete respectively. Integration of Eq. (23) yields the total amount of slip where we substitute Eqs. (20) and (21) as

$$u_s = \frac{L_s}{2E_s}\left(\sigma_h^s + \sigma_o^s\right) - \frac{L_s}{2E_c}\sigma_o^c \tag{24}$$

Stresses in concrete and steel at the end of debonded zone $\left(\sigma_o^s, \sigma_o^c\right)$ can be computed with the help of interfacial shear stress τ_s at the debonded interface which depends on the confinement, type of deformed bar, bar diameter and number of cycles in fatigue loading (Popov, 1984). Thus $\left(\sigma_o^s, \sigma_o^c\right)$ are determined by force balance in the free body of steel and surrounding fictitious concrete cylinder as

$$\sigma_o^s = \sigma_h^s - \frac{4L_s}{d_b}\tau_s \tag{25}$$

$$\sigma_o^c = \frac{d_b L_s}{h'\left(h' + d_b\right)}\tau_s \tag{26}$$

where h' is the radius of the fictitious concrete cylinder surrounding the rebar which is the minimum of clear cover, side cover and half of bar spacing.

COD profiles shown by the thin solid lines in Fig. 6 are drawn after adding slip of re-bars to the analytically computed COD profiles. It is assumed that the slip along re-bar periphery was uniform, increased towards the crack mouth and decreased towards the crack tip, both linearly with a slope of

$$\mu = \frac{u_s}{a - d_b - h}. \tag{27}$$

Thus the additives due to slip is zero at the crack tip, increases linearly to u_s at re-bar, constant within re-bar periphery and increases again with the same slope (Eq. 27) up to the crack mouth.

Strain correction

Since concrete carries a significant amount of stress at an uncracked section, strain gauge readings must be "corrected" before comparing with estimated strains obtained from inverse analysis at a cracked section. Strain gauges were attached 3 cm inward from the crack surface considering sensitivity of electrical resistance near the crack plane, which might lead to erroneous data or even damage due to progressive frictional stresses at rebar-concrete interface.

The lengths of debonded zones for all service loads were found smaller than 3 cm for the current RC beams. In such a condition, the concrete 'share' of stress is obtained from Eq. (25) as

$$\sigma_h^s - \sigma_o^s = \frac{4L_s}{d_b}\tau_s \tag{28}$$

and the strain correction is

$$\frac{\sigma_h^s - \sigma_o^s}{E_s} = \frac{4(1-\rho)}{E_s \pi^2 d_b^2 (1-\rho+n\rho)}\sigma_h^s \tag{29}$$

Appendix B: Weight function for an SEN specimen

The weight function for a SEN specimen of infinite length and finite width is (Tada et al., 1985)

$$G(x,a,b)=\frac{1}{\sqrt{\pi a}}\frac{g(x/a,a/b)}{\left(1-x^2/a^2\right)^{1/2}(1-a/b)^{3/2}} \tag{30}$$

where

$$g(x/a,\xi)=g_1(\xi)+\frac{x}{a}g_2(\xi)+\frac{x^2}{a^2}g_3(\xi)+\frac{x^3}{a^3}g_4(\xi) \tag{31}$$

$$g_1(\xi)=0.46+3.06\xi+0.84(1-\xi)^5+0.66\xi^2(1-\xi)^2 \tag{32}$$

$$g_2(\xi)=-3.52\xi^2 \tag{33}$$

$$\begin{aligned} g_3(\xi)=6.17-28.22\xi+34.54\xi^2-14.39\xi^3-(1-\xi)^{3/2} \\ -5.88(1-\xi)^5-2.64\xi^2(1-\xi)^2 \end{aligned} \tag{34}$$

$$\begin{aligned} g_4(\xi)=-6.63+25.16\xi-31.04\xi^2+14.41\xi^3+2(1-\xi)^{3/2} \\ -5.04(1-\xi)^5+1.98\xi^2(1-\xi)^2 \end{aligned} \tag{35}$$

Appendix C: Notations

The Following symbols are used in this paper

a = Crack length

b = Total depth of the beam (width of the fracture specimen)

d_b = Diameter of re-bar

E_c = Young's modulus of concrete

F_i = Total re-bars force in *i*-th layer of reinforcement

F = Total re-bars force in all the layers

f = Re-bar force simulated as force/unit length

G = Weight function for fracture specimens

g = Entries of the G matrix, approximated by it's finite difference equivalent

$H(\cdot)$ = Unit step function (Heaviside function)

h = Error in the approximation of the transformation

h_i = Clear distance from the bottom face of *i*-th re-bar layer

h_x = Step interval in discretization

L_2 = Linear space of square-integrable functions

L_s = The length of debonded zone

M = Applied moment on the crack plane

$M[\cdot]$ = The Tikhonov functional

n = Modular ratio

T = The transformation

T_h = The approximated transformation

U = Linear space where the crack closure vectors belong to

U_b' = Ultimate bond force per unit length between steel and concrete

u = Crack opening displacement

u_a = Crack opening due to the action of applied stress

u_b = Crack closing due to the action of re-bars force

u_s = Amount of slip between concrete and re-bar

x = Location along the crack (x', a' are dummy variable for x)

Z = Linear space where the re-bar force vectors belong to.

α = The regularization parameter

δ = Error in data

ν = Poisson's ratio

ρ = Reinforcement ratio

τ_s = Interfacial shear stress

σ = Applied stress

References

ACI. (1998). Nondestructive test methods for evaluation of concrete in structures. ACI 228. 2R-98. American Concrete Institute.

Bazant, Z.P., Cedolin, L., 1980. Fracture mechanics of concrete structures. Journal of the Engineering Mechanics Division, ASCE 106 (EM6), 1287 – 1306.

Bosco, C., Carpinteri, A., 1992. Fracture behavior of beams cracked along reinforcement. Theoretical and Applied Fracture Mechanics 17(1), 61-68.

Buchanan, D.J., John, R., Johnson, D.A., 1997. Determination of crack bridging stress from crack opening displacement profiles. International Journal of Fracture 87(2), 101-117.

Carpinteri, A., 1984. Stability of fracturing process in RC beams. Journal of Structural Engineering, ASCE 110(3), 544-558.

Carpinteri, A., 1991. Energy dissipation in R.C. beams under cyclic loadings. Engineering Fracture Mechanics 39(2), 177-184.

Carpinteri, A., Massabo, R., 1997. Continuous vs discontinuous bridged crack model for fiber reinforced materials in flexure. International Journal of Solids and Structures 34(18), 2321 – 2338.

Chong, K.P., Carino, N.J., Washer, G., 2003. Health monitoring of civil infrastructures. Smart Materials and Structures 12(3), 483 – 493.

Cox, B.N., Marshall, D.B., 1991a. Stable and unstable solutions for bridged crack in various specimens. Acta Metallurgica Materialia. 39(4), 579-589.

Cox, B.N., Marshall, D.B., 1991b. The determination of crack bridging forces. International Journal of Fracture 49(3), 159-176.

Fett, T., Munz, D., Seidel, J., Stech, S., Rodel, J., 1996. Correlation between long and short crack R-curves in Alumina using crack opening displacement and fracture mechanical weight function method. Journal of American Ceramic Society 79(5), 1189-1196.

Jenq, Y., Shah, S.P., 1991. Features of mechanics of quasi-brittle crack propagation in concrete." International Journal of Fracture 51(2), 103-120.

Kirsch, A., 1996. An introduction to the mathematical theory of inverse problems. Springer-Verlag New York, Inc.

Kitsutaka, Y., 1997. Fracture parameters by polylinear tension-softening analysis. Journal of Engineering Mechanics ASCE 123(5), 444-450.

Marshall, D.B., Cox, B.N., Evans, A.G., 1985. The mechanics of matrix cracking in brittle-matrix composites. Acta metallurgica 33(11), 2013-2021.

Massabo, R., Mumm D.R., Cox, B.N., 1998. Characterizing mode II delamination cracks in stitched composites. International journal of fracture 92(1), 1 – 38.

Nazmul, I.M., Matsumoto, T., 2003. Determination of steel stresses in reinforced concrete structures from crack opening profile. In: Proceedings of the 1st International conference on Structural Health Monitoring and Intelligent Infrastructure, Tokyo, Japan.

Nazmul, I.M., Matsumoto, T., 2004. Inverse analysis to determine re-bars' force from external crack opening measurements. Journal of Applied Mechanics JSCE 7, 1179 – 1186.

Nilson, A.H., Darwin, D., Dolan, C.W., 2003. Design of concrete structures, Thirteenth edition. McGraw Hill companies, Inc, NY.

Popov, E.P., 1984. Bond and anchorage of reinforcing bars under cyclic loading. ACI Journal Proceedings, 81(7-8), 340-349.

Rodel, J., Kelly, J.F., Lawn, B.R., 1990. In situ measurements of bridged crack interfaces in the scanning electron microscope. Journal of American Ceramic Society 73(11), 3313 - 3318.

Saouma, V. E., Ingraffea, A. R., Catalano, D. M., 1982. Fracture toughness of concrete: K_{IC} revisited. Journal of the Engineering Mechanics Division- ASCE 108(EM6), 1152-1167.

Schutter, G.D., 2002. Advanced monitoring of cracked structures using video microscope and automated image analysis. NDT & E International 35(4), 209-212.

Tada, H., Paris, P.C., Irwin, G.R., 1985. The stress analysis of cracks handbook. Paris Productions Inc., St. Louis, Missouri.

Tikhonov, A.N., Goncharsky, A.V., Stepanov, V.V., Yagola, A.G., 1990. Numerical methods for the solutions of ill-posed problems. Kluwer academic publishers group, Dordrecht, The Netherlands.

Fig. 1. Rebar forces are assumed as stepped functions

Fig. 2. Experimental set-up and specimen details

Fig. 3. Variation of rebar strain with total load in a sample test.

Fig. 4. Capturing digital images by a microscope

Fig. 5. Schematic explanation of image analysis (a) picture of a ruler showing 1 mm on the beam surface = 96 pixels on pictures (b) a sample picture (c) sample gray value profile and COD determination

Fig. 6. COD profiles on beam surface under a constant total load (inset).

Fig. 7. Sample rebar force by inverse analysis. Estimated rebar forces from solid profiles are in the insets to be compared with the Fig. 6 inset values.

Fig. 8. Length of debonded zone and assumed stresses at different points along the longitudinal direction of rebars.

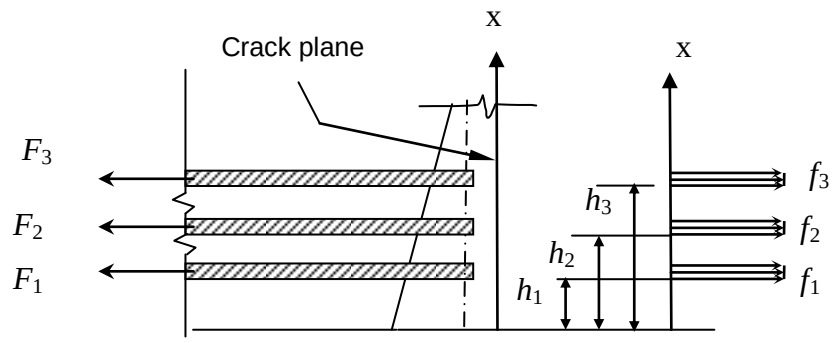

Fig. 1. Rebar forces are assumed as stepped functions

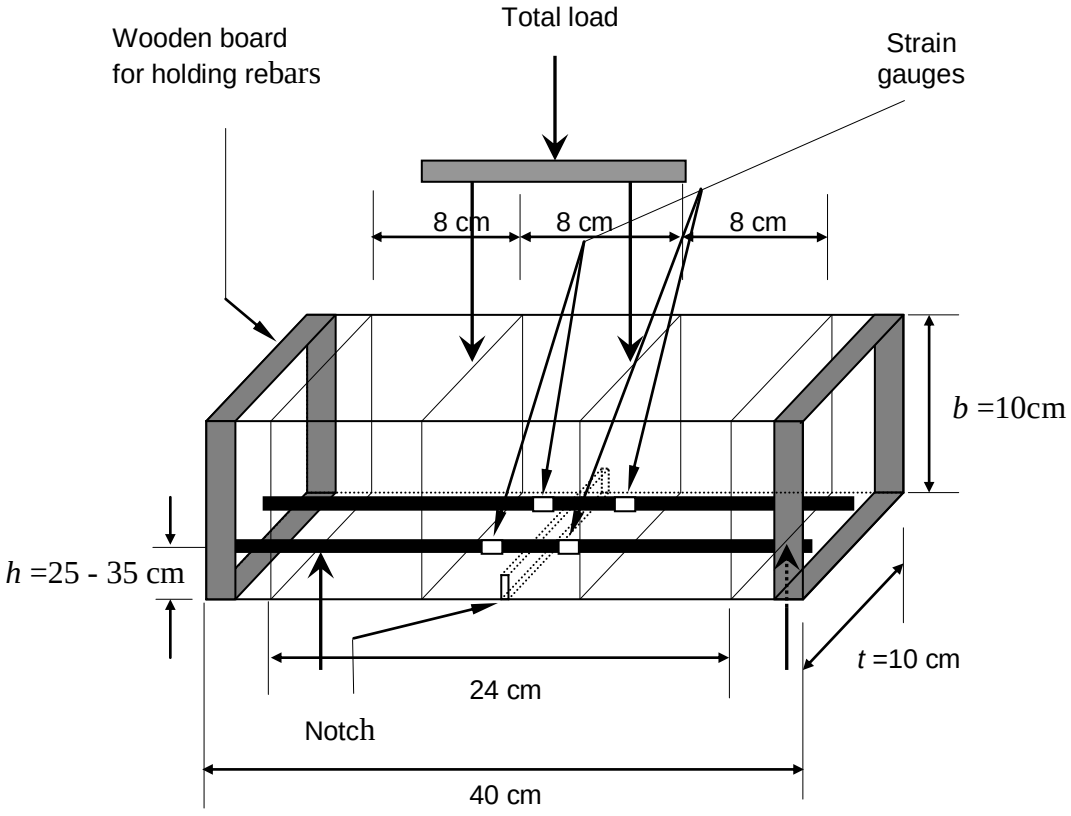

Fig. 2. Experimental set-up and specimen details

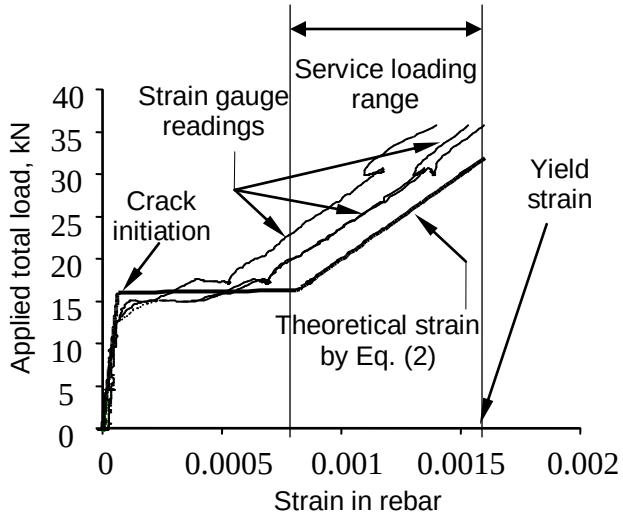

Fig. 3. Variation of steel strain with total load in a sample test.

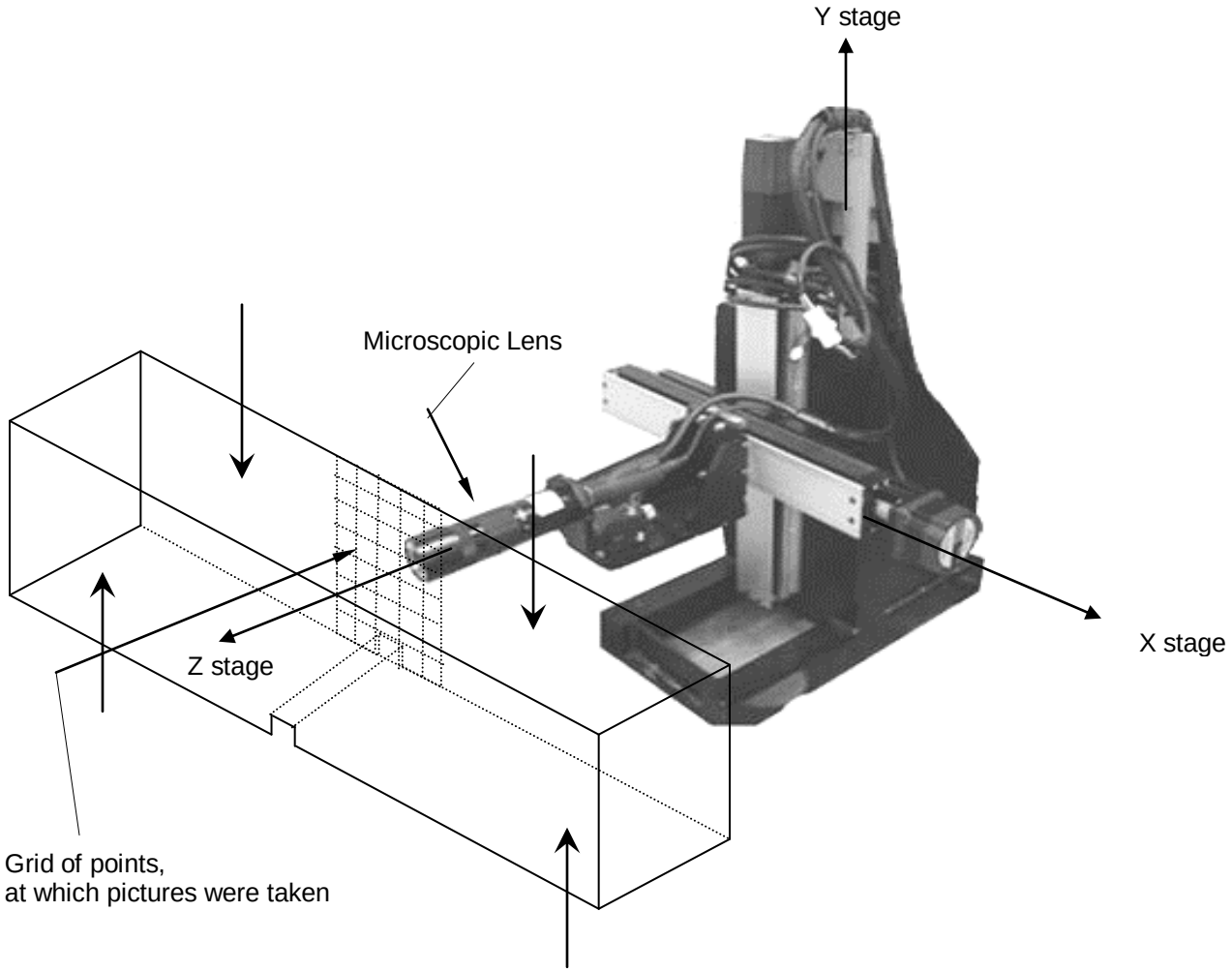

Fig. 4. Capturing digital images by a microscope

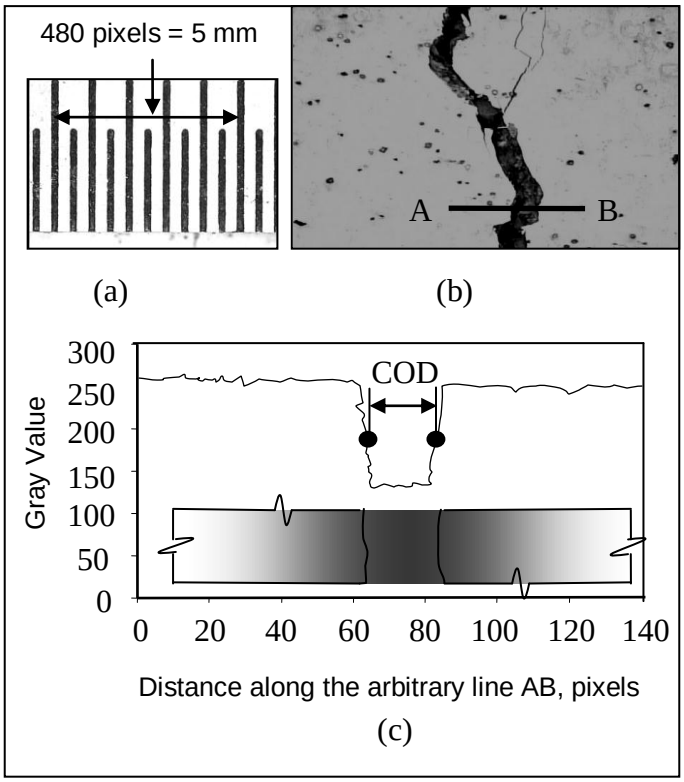

Fig. 5. Schematic explanation of image analysis (a) picture of a ruler showing 1 mm on the beam surface = 96 pixels on pictures (b) a sample picture (c) sample gray value profile and COD determination

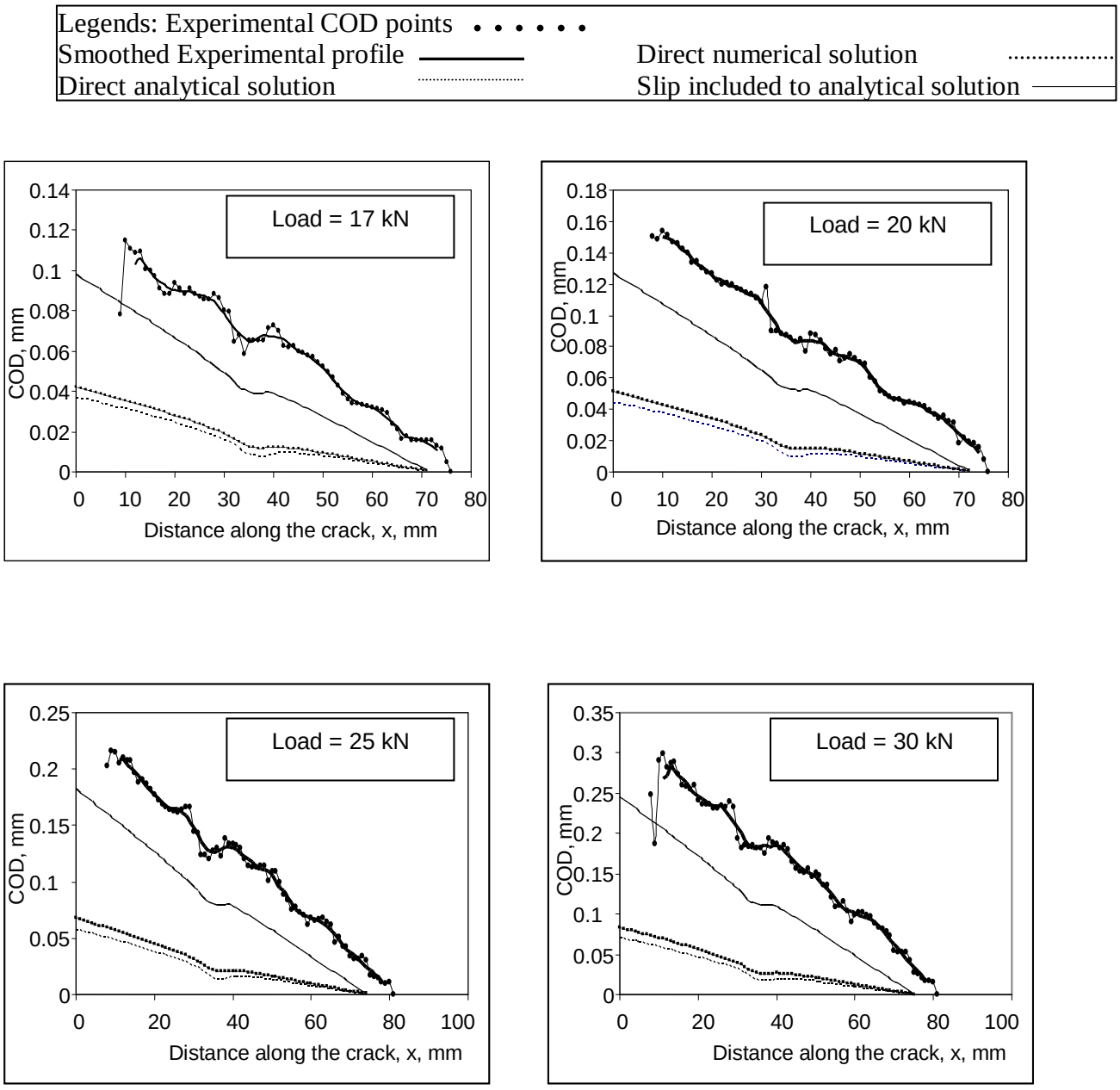

Fig. 6. COD profiles on beam surface under a constant total load (inset).

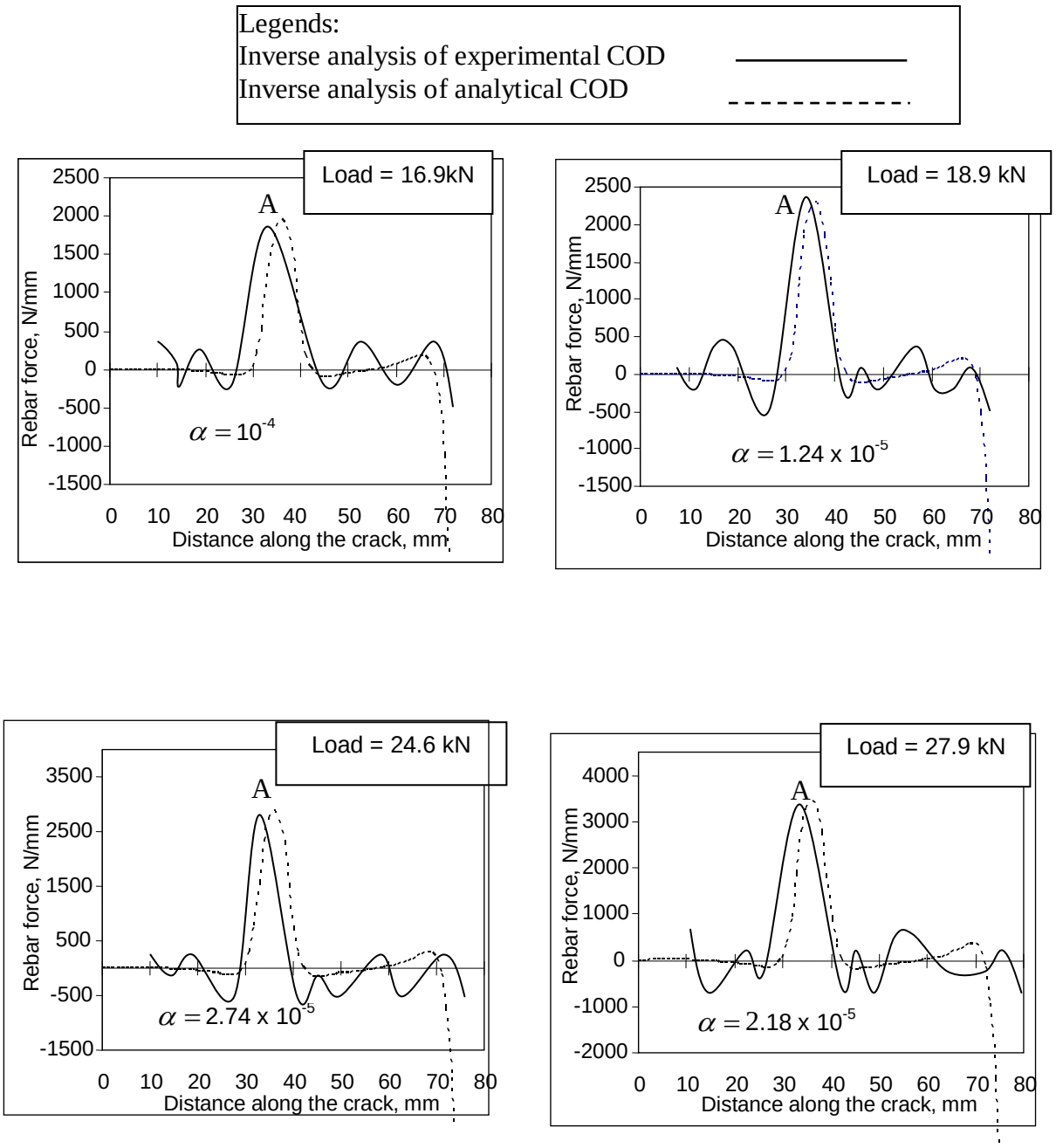

Fig. 7. Sample rebar forces by inverse analysis with $h = 10^{-3}$. Estimated rebar forces from solid profiles are in the insets, to be compared with the Fig. 6 inset values.

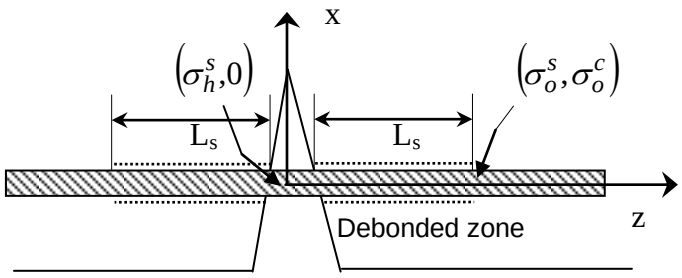

Fig. 8. Length of debonded zone and assumed stresses at different points along the longitudinal direction of rebars.

Table 1: Applicability of the inverse analysis method for measuring reinforcing steel stress/strain compared with other methods.

Sample specimen : cross-section 10cm x 10cm, span:24 cm, clear cover: 3.3 cm										
Load	Bending Moment at Mid-section	Re-bar Stress			Errors in re-bar stress from inverse analysis		Re-bar Strain			Errors in re-bar strain from inverse analysis 100(Y-C-D)/ Y
		Inverse analysis (X)	Section analysis[1] (A)	Fracture analysis[2] (B)	Compared with section analysis 100(X-A)/A	Compared with fracture analysis 100(X-B)/B	Inverse analysis (Y)	Gauge reading (C)	Strain Correction[3] (D)	
Ton	N-mm	MPa	MPa	MPa	%	%	μm/mm	μm/mm	μm/mm	%
1.7	677262	220	209.3	232	4.86	-5.45	1.1	0.698	0.264	12.54
2.02	804747	258	248.7	280	3.60	-8.53	1.29	0.854	0.284	11.78
2.51	999958	324	309.03	334	4.62	-3.09	1.62	1.113	0.325	11.23
3.02	1.203×10^6	384	371.9	402	3.15	-4.69	1.92	1.444	0.338	7.18

[1] Based on Eq. (2).

[2] Based on fracture analysis by Bosco and Carpinteri (1992).

[3] A good percentage of total tensile stress is carried by concrete at un-cracked section where strain gauges were attached.